Dissociative recombination in xenon: Variation of the total rate coefficient and excited-state production with electron temperature

Yueh-Jaw Shiu, Manfred A. Biondi, and Dwight P. Sipler
Department of Physics and Astronomy, University of Pittsburgh, Pittsburgh, Pennsylvania 15260
(Received 22 October 1976)

A three-mode microwave afterglow apparatus has been used in conjunction with a high-speed grating spectrometer to study the variation with electron temperature of the recombination coefficient $\alpha(Xe_2^+)$ and of the Xe* excited states produced by dissociative recombination over the range $300 \leq T_e \leq 8000$ K. At low electron temperatures, 300–700 K, $\alpha(Xe_2^+)$ varies approximately as $T_e^{-1/3}$, with a smooth transition to a $\sim T_e^{-0.7}$ variation at higher electron temperatures, 1300–7400 K. At $T_e = T_+ = T_n = 300$ K, $\alpha(Xe_2^+) = (2.3 \pm 0.2) \times 10^{-6}$ cm^3/sec, in agreement with earlier studies at room temperature. At thermal energy (300 K) Xe* excited states up to but not exceeding the energy of the Xe_2^+ ion in its ground electronic and vibrational state are observed. With microwave heating to $T_e \sim 8000$ K additional, higher-lying Xe* states (up to ~0.6 eV above the Xe_2^+ ion ground state) are produced by the dissociative recombination process.

I. INTRODUCTION

The study of recombination between Xe_2^+ ions and electrons as the electron temperature is varied is of interest because (a) it offers insight into the dissociative recombination mechanism for a simple diatomic ion containing many electrons and (b) it provides needed information concerning the overall recombination rate and the formation of particular excited states under conditions of interest for the xenon plasmas of certain excimer and rare-gas–alkali-halide lasers. In the present case the dissociative recombination reaction under study is

$$Xe_2^+ + e^- \rightleftharpoons (Xe_2)_u^* \rightarrow Xe^* + Xe\,, \tag{1}$$

where the superscript * indicates an electronically excited state and the subscript u indicates an unstable (i.e., repulsive) molecular state.

The rate coefficient $\alpha(Xe_2^+)$ for the overall process has been obtained at room temperature, $T_e = T_+ = T_n = 300$ K (the subscripts e, $+$, and n indicate electron, positive ion, and neutral gas, respectively) by several investigators[1-3]; also, the excited states produced by recombination at room temperature have been studied recently.[4] In the present investigations microwave afterglow techniques employing microwave heating of the electrons have been used to extend the electron temperature range over which the recombination is studied from 300 to ~8000 K.

II. METHOD OF MEASUREMENT AND ANALYSIS

The microwave afterglow apparatus, which employs a high-Q TM_{010} cavity mode for plasma generation and for electron concentration determinations and a TE_{11} circular wave guide mode for electron heating (see Fig. 1), has been described in detail previously.[5] The quartz bottle containing the plasma afterglow is a circular cylinder (with tapered ends) of radius 1.5 cm and effective length 9.1 cm and is connected to an ultrahigh-vacuum gas-handling system. The xenon gas is research grade from Linde Division of Union Carbide Corp. In the present experiment the discharge (plasma generation) typically lasts 0.5 msec and is repeated at a 30-Hz rate.

The decay of electron concentration during the afterglow is obtained from measurements of the cavity's resonant frequency shift, from which one calculates $\bar{n}_{\mu w}$, the "microwave-averaged" electron density.[5] The recombination coefficient $\alpha(Xe_2^+)$ is obtained by comparing the observed $\bar{n}_{\mu w}(t)$ values with those obtained by computer solution of the electron continuity equation,[5]

$$\frac{\partial n_e(\vec{r}, t)}{\partial t} \simeq -\alpha n_e^2 + D_a \nabla^2 n_e\,, \tag{2}$$

appropriate for a recombination-dominated afterglow with only one ion species (i.e., Xe_2^+) of importance, so that $n_e \simeq n_+$. D_a is the ambipolar dif-

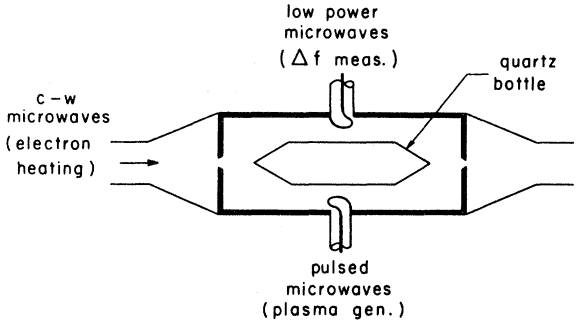

FIG. 1. Schematic diagram of the microwave resonant cavity-waveguide afterglow apparatus.

fusion coefficient of Xe_2^+ ions and electrons and may be calculated from the relation $D_a = D_+(1 + T_e/T_+)$, with D_+ obtained from the measured ion mobility of Xe_2^+ in Xe.[6] At the xenon pressures used in the present experiment, 5–20 Torr, the loss of electrons by recombination greatly outweighs ambipolar diffusion loss (except at the highest T_e values studied); however the second term on the right of Eq. (2) has a pronounced effect on the spatial distribution of the electrons in the quartz bottle and therefore affects the calculated values of $\bar{n}_{\mu w}(t)$. Since the solution of Eq. (2) in the limit of small diffusion loss is the well-known "recombination decay," $1/n_e(\vec{r}, t) = 1/n_e(\vec{r}, 0) + \alpha t$, we present our data as plots of $1/\bar{n}_{\mu w}(t)$ vs t.

At the microwave frequency ($\omega = 1.93 \times 10^{10}$ Hz) and xenon pressures of 5–20 Torr used in the present experiment the frequency shift data must be corrected for finite collision frequency (ν_c) effects in order to obtain the $\bar{n}_{\mu w}$ values. Approximating the observed variation[7] with electron energy by $\nu_c(\text{sec}^{-1}) \simeq 3 \times 10^8 [p(\text{Torr})][u_e(\text{eV})]^{-1/2}$ for the electron temperature range of interest, increases in the $\bar{n}_{\mu w}$ values ranging from 15% at 5 Torr to 240% at 20 Torr are obtained compared to the $\nu_c/\omega \ll 1$ case.

The optical radiation emitted from the afterglow is monitored by means of a Spex Model 1500 SP Grating Spectrometer employing an EMI 9658A photomultiplier operated in a pulse-counting mode. The range of wavelengths detectable with the present optics and photomultiplier is from ~3900 to ~8800 Å. In order to obtain a wavelength scan of the radiation emitted at a particular time in the afterglow, the wavelength drive of the spectrometer is run at typically 20 Å/min, and the amplifiers in the pulse-counting electronics are gated on for the selected afterglow interval. The pulses during this interval are fed to a digital rate meter with an averaging time for the analog output of typically 1 sec. The output is fed to a chart recorder.

When the afterglow spectrum has been characterized, the variation of the intensity of a particular line during the afterglow is studied by setting the spectrometer to the appropriate wavelength and feeding the photomultiplier output pulses to a 100-channel multichannel analyzer operating in a multiscaling mode. The start of the multichannel analyzer sweep is synchronized with the start of each afterglow, with a typical dwell time per channel of 100 μsec.

III. RESULTS

Examples of the $1/\bar{n}_{\mu w}$ vs t data obtained in xenon at 5 Torr are shown for various values of T_e in Fig. 2. The solid lines represent the best fits to the data of the computer solutions of Eq. (2) treating α as a parameter. (No attempt has been made to fit to the early time data, when metastable-metastable ionization effects are apparent.) The pronounced upward curvature of the curves at late times and higher T_e values indicates the increasing importance of ambipolar diffusion loss. In a test for a possible pressure dependence of the recombination coefficient, no systematic variation (<2%) in the inferred α values was found over the xenon pressure range 5–20 Torr at $T_e = T_+ = T_n = 300$ K.

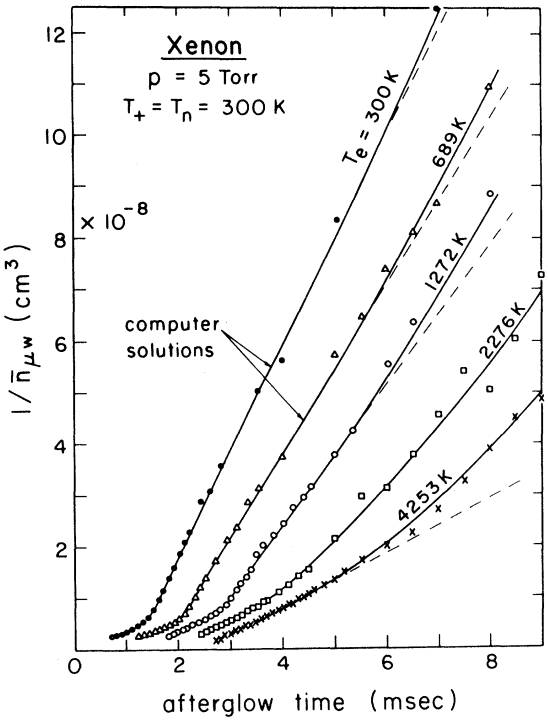

FIG. 2. Plots of the reciprocal of the "microwave-averaged" electron density versus time, with T_e as a parameter. The zero afterglow times of successive curves are displaced by 0.5 msec for clarity. The solid lines represent fits to the data of solutions of Eq. (2).

The values of $\alpha(Xe_2^+)$ vs T_e inferred from the data of Fig. 2 are shown in Fig. 3. A smooth decrease of α with increasing T_e is noted, the dependence on T_e becoming stronger above ~1000 K, where the variation can be represented by $\alpha \sim T_e^{-0.72}$.

In order to determine which excited states of Xe are produced by the dissociative recombination of Xe_2^+ ions and electrons, the decays of the afterglow radiation intensity and of the electron concentration are compared. For two-body recombination production of the excited states it is readily shown that the emission intensity I resulting from

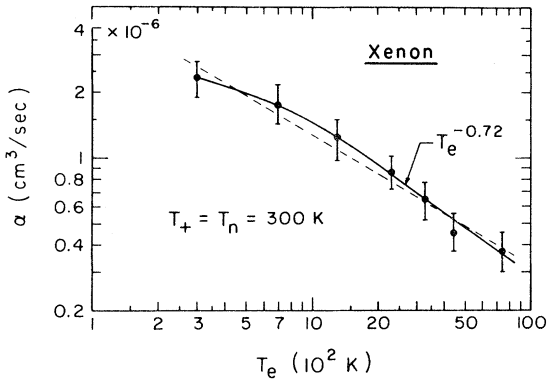

FIG. 3. Variation of $\alpha(Xe_2^+)$ with electron temperature at $T_+ = T_n = 300$ K.

radiative decay of such excited states varies as n_e^2. Therefore, in Fig. 4 we have compared relative variations of $I^{1/2}$ and n_e for three representative transitions, 8280 Å ($6p_{00}$-$6s_{11}$), 7642 Å ($6p'_{01}$-$6s'_{00}$), and 4671 Å ($7p_{23}$-$6s_{12}$) (modified Racah notation). It will be seen that in these cases the predicted dependence of intensity on n_e is verified. Other transitions, such as 6872 Å ($6f_{45}$-$5d_{34}$) and 7120 Å ($7d_{34}$-$6p_{23}$) die out very quickly (decay time constants ~100 μsec). The positions of these and other transitions on a partial energy-level diagram of xenon are shown in Fig. 5.

In the case of no microwave heating, $T_e = T_+ = T_n = 300$ K, the following transitions indicate a time decay appropriate to a recombination origin (ranked in order of decreasing intensity): 8280 Å ($6p_{00}$-$6s_{11}$), 8232 ($6p_{12}$-$6s_{12}$), 7642 ($6p'_{01}$-$6s'_{00}$), 8347 ($6p'_{12}$-$6s'_{01}$), 8819 ($6p_{23}$-$6s_{12}$), 7967 ($7p_{11}$-$6s'_{00}$), 7887 ($6p'_{00}$-$6s'_{01}$), 8206 ($6p'_{11}$-$6s'_{00}$), 8267 ($6p'_{01}$-$6s'_{01}$), 8409 ($6p_{11}$-$6s_{12}$), 4671 ($7p_{23}$-$6s_{12}$), 4624 ($7p_{12}$-$6s_{12}$), 4923 ($7p_{22}$-$6s_{11}$), 4734 ($6p'_{12}$-$6s_{11}$), 4807 ($7p_{00}$-$6s_{11}$), 4830 ($7p_{11}$-$6s_{11}$), 4843 ($7p_{12}$-$6s_{11}$), 4917 ($6p'_{11}$-$6s_{11}$), 4697 ($7p_{22}$-$6s_{12}$), 4501 ($6p'_{01}$-$6s_{12}$), 4525 ($6p'_{12}$-$6s_{12}$), and 4583 ($6p'_{00}$-$6s_{11}$).

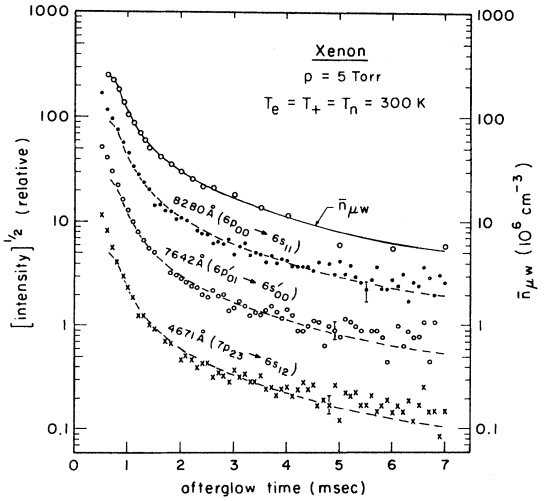

FIG. 4. Comparison of the decay of electron density $\bar{n}_{\mu w}(t)$ and the square root of the afterglow intensity $I^{1/2}$ of selected afterglow transitions for the case $T_e = T_+ = T_n = 300$ K. The dashed curves through the $I^{1/2}$ data represent the renormalized $\bar{n}_{\mu w}$ data.

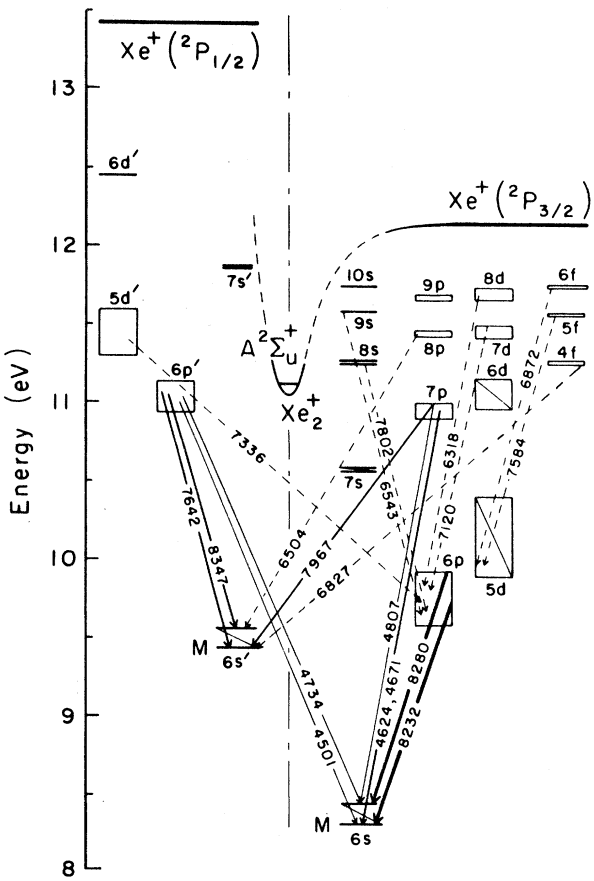

FIG. 5. Partial energy level diagram for xenon showing typical transitions observed to result from dissociative recombination of Xe_2^+ ions and electrons. Solid lines, unheated case ($T_e = T_+ = T_n = 300$ K). Dashed lines, additional transitions resulting from recombination with heated electrons ($T_e \sim 8000$ K). The weights of the lines indicate qualitatively the observed emission intensities. A diagonal line through a state indicates that transitions from that state were unobservable with the present apparatus.

When microwave heating to $T_e \sim 8000$ K is employed, additional transitions are found to result from electron-ion recombination in the afterglow, (again, ranked in order of decreasing intensity): 7120 Å ($7d_{34}$-$6p_{23}$), 6882 ($7d_{33}$-$6p_{22}$), 6827 ($4f_{11}$-$6s'_{00}$), 7584 ($5f_{45}$-$5d_{34}$), 7802 ($8s_{11}$-$6p_{22}$), 7394 ($7d_{23}$-$6p_{12}$), 6872 ($6f_{45}$-$5d_{34}$), 7336 ($5d'_{23}$-$6p_{22}$), 6318 ($8d_{34}$-$6p_{23}$), 6543 ($9s_{12}$-$6p_{22}$), and 6504 ($8p_{00}$-$6s'_{01}$).

IV. DISCUSSION AND CONCLUSIONS

A. Total recombination coefficient

At $T_e = T_+ = T_n = 300$ K the present studies yield the value $\alpha(Xe_2^+) = (2.3 \pm 0.2) \times 10^{-6}$ cm^3/sec. This value is in excellent agreement with that of Lennon and Sexton[2] but is about 60% higher than the value obtained by Oskam and Mittelstadt.[3] We cannot account for the discrepancy with the latter work; the xenon used in the present work is free of contaminants which might significantly affect the electron loss rate (i.e., nitrogen, the most significant impurity, is present at a level of $\lesssim$10 ppm). Also, only xenon lines are observed in the afterglow, although this is not a sufficient condition for demonstrating the absence of impurities.

The large value of $\alpha(Xe_2^+)$ continues the trend, observed for the noble-gas ions He_2^+ through Kr_2^+, of an increase in α with increasing number of electrons in the atoms making up the diatomic ion.[8] It is to be expected that, for cases in which stabilization by dissociation greatly outweighs the likelihood of autoionization of the intermediate complex [see Eq. (1)], the increase in initial capture cross section with increasing complexity of the diatomic ion results in a corresponding increase in the recombination coefficient for the overall process.[9]

If one chooses to represent the observed variation of $\alpha(Xe_2^+)$ with T_e shown in Fig. 3 by a single-term power-law dependence, then a least-squares fit to the data yields the result, $\alpha(\text{cm}^3/\text{sec}) = 2.66 \times 10^{-7} [300/T_e(\text{K})]^{0.60}$. This variation, indicated by the light dashed line in the figure, lies close to the usual $T_e^{-1/2}$ variation predicted[9] for the direct dissociative process involving a single potential curve crossing between the initial and intermediate states indicated in Eq. (1). However, the error bars shown in Fig. 3 largely represent systematic errors, so that the relative variation of $\alpha(Xe_2^+)$ with T_e is probably more nearly that shown by the solid line, which tends to a $T_e^{-0.72}$ dependence above ~1000 K.

The faster-than-$T_e^{-1/2}$ variation may result from the fact that the time for stabilization by dissociation increases with increasing electron energy, so that the probability of autoionization is no longer negligible compared to dissociation at higher energies, and therefore the overall recombination rate becomes less than the initial capture rate. However, an offsetting effect occurs if additional potential curve crossings come into play at higher electron energies. In this case new final states become accessible at higher electron energies, and the overall variation of α with T_e may tend to be slower than for the case of a single curve crossing. In Sec. IV B, we discuss evidence for additional recombination channels at higher electron energies.

B. Excited states produced by recombination

The transitions observed to originate from electron-ion recombination during the afterglow have been given in Sec. III, and the majority are shown in Fig. 5. The energy levels in the figure are designated in modified Racah notation, the unprimed and primed states converging, respectively, to the $^2P_{3/2}$ and $^2P_{1/2}$ levels of the Xe^+ ion's doublet ground state. The solid lines indicate transitions observed with no microwave heating; the dashed lines represent additional transitions observed with electron heating up to $T_e \sim 8000$ K.

It will be seen that, in the absence of electron heating, no final states of Xe* are produced which lie above the $v = 0$ vibrational level of the Xe_2^+ ($A\,^2\Sigma_u^+$) ion ground state.[10,11] This observation is consistent with formation of the excited states by dissociative recombination of thermal electrons with ground state (electronic and vibrational) Xe_2^+ ions. The observation of $6p$, $7p$, and $6p'$ Xe* final states may indicate multiple favorable crossings of the potential curves of the $(Xe_2^+ + e)$ initial state and the various $(Xe_2^*)_u$ intermediate states [refer to Eq. (1)], as might be expected for a complicated atomic system such as Xe.

With electron heating to mean energies approaching 1 eV, additional Xe* excited states, lying as much as ~0.6 eV above the Xe_2^+ ion ground state, are observed. This finding is also consistent with the dissociative recombination process, in which repulsive potential curves of Xe_2^* states which cross the $(Xe_2^+ + e)$ state well above its minimum become accessible when the incoming electron has sufficient kinetic energy to reach these states.

Our observations are consistent with the production by dissociative recombination of any final state which lies lower in energy than the initial $(Xe_2^+ + e)$ state, independent of the particular quantum numbers of that state. Within our wavelength detection limits, we observe all possible Xe* final states, whether they belong to the $^2P_{3/2}$ ground state of the Xe^+ ion core or to the $^2P_{1/2}$ ion core. Since the electronic wave function of the Xe_2^+ ion is an admixture of $^2P_{3/2}$ and $^2P_{1/2}$ contributions, final states of Xe* belonging to either of these ion core states are allowed.

ACKNOWLEDGMENTS

The authors are indebted to J. N. Bardsley for helpful discussions of the theory of the dissociative recombination process. This research was supported, in part, by the Advanced Research Projects Agency of the Department of Defense and was monitored by ONR under Contract No. N00014-76-C-0098.

[1]J. M. Richardson, Phys. Rev. 88, 895 (1952).
[2]J. J. Lennon and M. C. Sexton, J. Electron. Control 7, 123 (1959).
[3]H. J. Oskam and V. R. Mittelstadt, Phys. Rev. 132, 1445 (1963).
[4]A. Barbet, N. Sadeghi, and J. C. Pebay-Peyroula, J. Phys. B 8, 1785 (1975).
[5]L. Frommhold, M. A. Biondi, and F. J. Mehr, Phys. Rev. 165, 44 (1968).
[6]See, for example, E. W. McDaniel and E. A. Mason, *The Mobility and Diffusion of Ions in Gases* (Wiley, New York, 1973).
[7]A. L. Gilardini, *Low Energy Electron Collisions in Gases* (Wiley, New York, 1973).
[8]M. A. Biondi, Comments Mod. Phys. D4, 85 (1973).
[9]J. N. Bardsley and M. A. Biondi, in *Advances in Atomic and Molecular Physics*, edited by D. R. Bates (Academic, New York, 1970), Vol. 6.
[10]R. S. Mulliken, J. Chem. Phys. 52, 5170 (1970).
[11]J. A. R. Sampson and R. B. Cairns, J. Opt. Soc. Am. 56, 1140 (1966).